SCIENTIFIC REPORTS

OPEN

SUBJECT AREAS:
FLUORESCENCE IMAGING
DRUG DELIVERY
NANOPARTICLES
CHEMOTHERAPY

Received
24 May 2013

Accepted
24 September 2013

Published
24 October 2013

Correspondence and requests for materials should be addressed to Y.W. (wuy@nanoctr.cn) or X.J.L. (liangxj@nanoctr.cn)

* These authors contributed equally to this work.

Ultrabright and Multicolorful Fluorescence of Amphiphilic Polyethyleneimine Polymer Dots for Efficiently Combined Imaging and Therapy

Yun Sun[1,2]*, Weipeng Cao[1]*, Shengliang Li[1], Shubin Jin[1], Kelei Hu[1,2], Liming Hu[2], Yuanyu Huang[3], Xueyun Gao[4], Yan Wu[1] & Xing-Jie Liang[1]

[1]Chinese Academy of Sciences Key Lab for Biological Effects of Nanomaterials and Nanosafety, National Center for Nanoscience and Technology No.11, First North Road, Zhongguancun, Beijing 100190, P.R. China, [2]College of Life Science and Bioengineering Beijing University of Technology No.100 Pingleyuan, Chaoyang District, Beijing 100124, P.R.China, [3]Laboratory of Nucleic Acid Technology, Institute of Molecular Medicine, Peking University, 5 Yiheyuan Road, Beijing 100871, P.R.China, [4]CAS Key Laboratory for Biomedical Effects of Nanomaterials and Nanosafety, Institute of High Energy Physics, Chinese Academy of Sciences, Beijing, 100049, P.R. China.

Multifunctional nanoparticles as theranostic tools hold great potential for its unique and efficient way to visualize the process of disease treatment. However, the toxicity of conventional fluorescent labels and difficulty of functionalization limit their widespread use. Recently, a number of amino-rich polymers have demonstrated high luminescent fluorescence but rarely showed potential for in vivo imaging due to their blue fluorescence. Here, a general route has been found to construct polymer-based multifunctional nanoparticles for combined imaging and drug delivering. The weak fluorescent polyethyleneimine (PEI) has been conjugated with hydrophobic polylactide as the amphiphilic PEI for construction of nanoparticles which showed bright and multicolor fluorescence with high drug loading capacity. The paclitaxel-loaded nanoparticles showed significant therapy effect in contrast to the free paclitaxel. Meanwhile, fluorescence imaging of the nanoparticles showed accumulation around tumor. These results demonstrate a new type of polymer-based multifunctional nanoparticles for imaging-guided drug delivery.

There has been intense interest in the development of nanomaterials as therapeutic and diagnostic agents, owing to their unique properties including large, specific drug loading capacity[1], strong superparamagnetism[2], or efficient photoluminescence[3]. Recently, a number of nanomaterials have been constructed for use in imaging or therapy systems, such as polymeric nanoparticles[4], quantum dots[5], gold nanoparticles[6], and paramagnetic nanoparticles[7]. Among these, only biocompatible polymeric nanoparticles that can encapsulate hydrophilic or hydrophobic drugs have been approved for clinical application[8]. However, polymer-based nanoparticles generally require the introduction of an additional molecular tag so that drug delivery can be monitored *in vivo*[9]. Owing to their unique optical properties, quantum dots are often conjugated with polymeric nanoparticles for use in combined imaging and therapy[10], but the intrinsic toxicity of such materials has limited their further application and clinical translation[11]. Nevertheless, luminescent polymer dots (PDs), which are biocompatible and brightly fluorescent, have recently been used as labels for biological imaging[12,13]. However, PDs are difficult to functionalize with biological molecules or conjugate with drug delivery vehicles. Phospholipid encapsulation[14] or blending with functional polymers[15,16] can overcome this problem, but the introduction of additional polymers or nanoparticles makes the PDs less effective[17] and results in alteration of the emission sensitivity[14]. Therefore, luminescent PDs with the potential for drug delivery without further modification would be highly desirable.

Here we developed novel, multifunctional PDs which can encapsulate drugs and act as an imaging tag. The PDs were produced from an amphiphilic polymer based on polyethyleneimine (PEI) and hydrophobic polylactide (PLA) (Fig. 1a). Drugs can be easily encapsulated into the PDs through a modified emulsion/evaporation method.

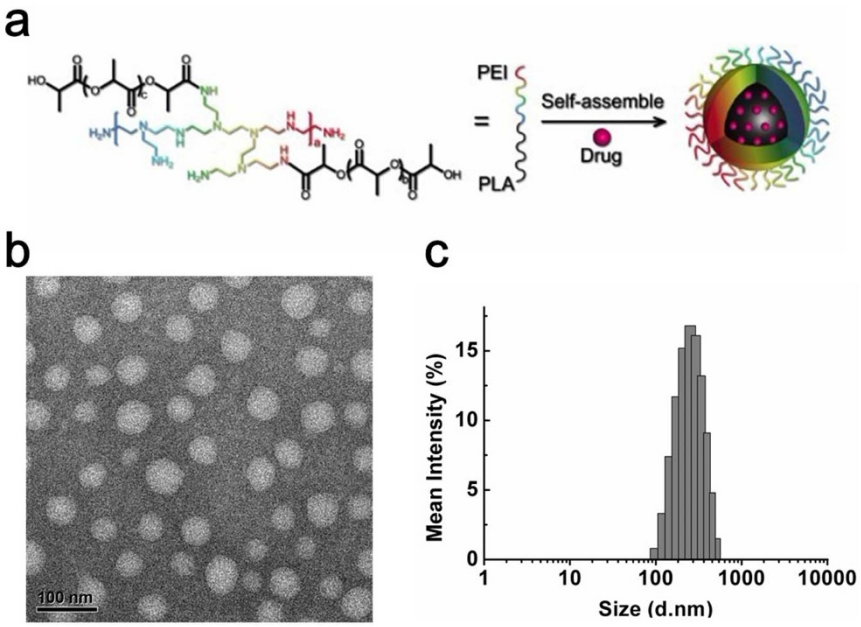

Figure 1 | (a) Schematic illustration of the construction of the multifunctional PDs. (b,c) TEM and DLS characterization of blank PDs. Scale bar, 100 nm.

Moreover, the PDs possess an unexpectedly bright, multicolor fluorescence in comparison to the weak fluorescence of PEI alone. Most importantly, due to the unique proton sponge effect of PEI, the drug-loaded PDs effectively overcame a major hurdle for drug delivery vehicles[18,19] by escaping from endosomes/lysosomes into the cytoplasm. In addition, the drug-loaded PDs have higher antineoplastic activity compared with free drug. Hence, PDs derived from amphiphilic PEI could be ideal theranostic tools for imaging-guided drug delivery.

Results

Synthesis and characterization of PEI-PLA copolymers. The amphiphilic copolymer was constructed by conjugating the PEI with hydrophobic PLA using a one-step ring-opening polymerization method as previously described with some changes[20] (Scheme S1). We synthesized a series of copolymers with different weight ratios of D, L-lactide/PEI. A weight ratio of 60 gave a copolymer which had the optimal balance of hydrophobic and hydrophilic segments and could potentially form well-defined, uniform nanoparticles. This copolymer was therefore selected for further research. FT-IR and ^{1}H NMR spectra are shown in Fig. S1. The molecular weight of the final amphiphilic polymer was 127 kDa and the polydispersity (Mw/Mn) was 1.50.

Preparation and characterization of PDs. PDs were then constructed using a modified emulsion/solvent evaporation technique as previously reported[21]. The PDs were well-dispersed with a typical spherical shape and a size around 50 nm (Fig. 1b). The hydrodynamic size of the PDs in phosphate buffer solution was 226.7 $\pm$ 3.1 nm by dynamic light scattering (DLS) (Fig. 1c). The zeta potential was 11.1 $\pm$ 0.5 mv, and the positive charge was much lower than PEI (reported as $\sim$50 mv[22]) because the amino groups of the PEI in the PDs were partly reacted with the PLA.

The as-synthesized PDs exhibited extraordinarily bright and colorful fluorescence in aqueous solution (Fig. 2a, b). At an emission wavelength of 450 nm, the fluorescence quantum yield (QY) of the PDs was as high as 0.31, compared with the previously reported QY of 0.01 for PEI[23]. Moreover, the emission spectra of the PDs were generally broad and were sensitive to the excitation wavelengths (Fig. 2a, b). When the solution of PDs was excited at wavelengths from 360 to 540 nm, the emission peak shifted from 450 nm to 615 nm and the fluorescence intensity decreased remarkably. More importantly, as can be seen from Fig. 2b, the normalized spectra clearly indicate that the emission peaks shift to red and near-infrared windows as the excitation wavelength increases, a property which may be suitable for *in vitro* and *in vivo* imaging. The similar excitation-dependent fluorescence behavior was also observed from the solution of PEI (Fig. S2). However, unlike the significant red-shift of PDs, PEI showed negligible fluorescence when excited at wavelengths above 420 nm and thus resulted in no obvious visible green fluorescence. We then investigated the fluorescent lifetime of the PDs using a time-correlated single-photon counting instrument (Fig. 2c). The average lifetime is 3.1 ns and contains two components with different ratios, 4.8 ns ($\sim$56%) and 1.0 ns ($\sim$44%), and no multi-electron trapping was observed. The fluorescence of PDs in solution was ten times higher than the copolymer solution (Fig. 2d). When irradiated by UV light at 360 nm, powdered PEI-PLA copolymer exhibited significant white fluorescence while Rhodamine B powder gave negligible luminescence (Fig. S3). Interestingly, we show that the PEI-based PDs show significant pH-dependent fluorescence (Fig. S4). When the aqueous solution of the PDs changed from acidic (pH 2) to basic environment (pH 14), the fluorescence intensity decreased obviously both at the emission of 450 nm and 540 nm. As can be seen from Fig. S4, the enhanced fluorescence at pH 2 could be attributed to the much more compact structure of PDs.

To further optimize the production process of the multicolour of PDs. The reaction solution of PEI-PLA at different interval time was collected (Fig. S5). The emission intensity excited at 320 nm went up with the increase of the ratio of PLA segment. Meanwhile, the emission was enhanced and red-shift to 500 nm with increasing reaction time. Taken together, we demonstrate that the rigid structure of PEI-PLA and much more compact structure of PDs resulted in the aggregation-enhanced emission and red-shift of fluorescence[24].

Biocompatibility of PDs. The biocompatibilities of PDs were investigated using a CCK-8 assay in human breast cancer MCF-7 cells (Fig. 3a). PDs were much less cytotoxic than PEI. Although cytotoxicity of the PDs increased slightly with increasing concentration, the concentrations of PDs used in the *in vitro* evaluations were significantly higher than those required for applications such as

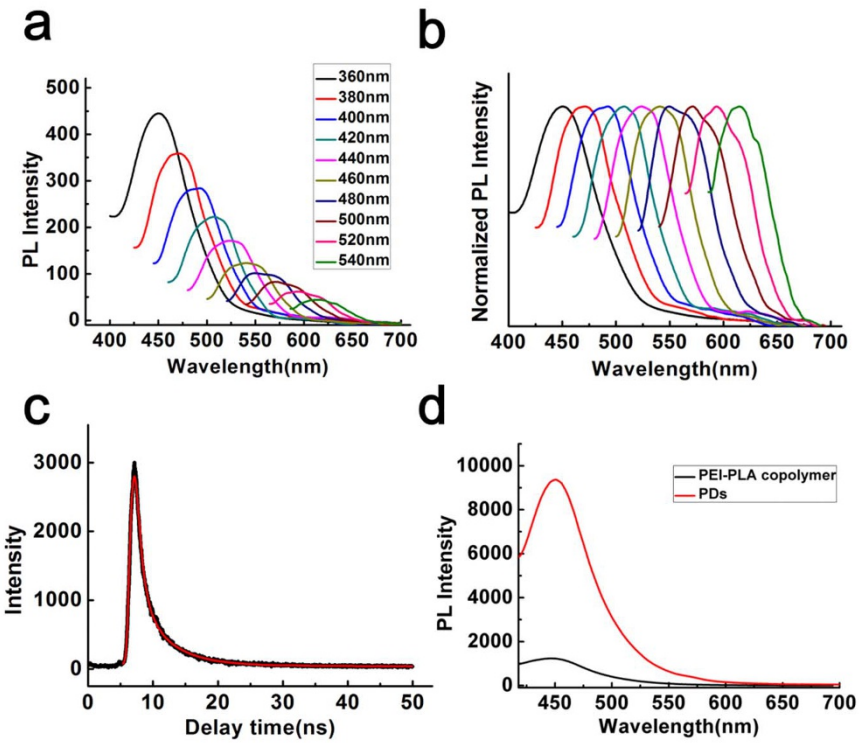

Figure 2 | (a, b) Luminescence emission spectra (with progressively longer excitation wavelengths in 20 nm increments from 360 nm on the left) (a) and normalized emission spectra with the same excitation wavelengths (b). (c) Fluorescence lifetime of PDs. (d) Fluorescence intensity of PEI-PLA copolymer and PDs at the same concentration.

optical imaging of living cells. Because the PDs were designed for intravenous administration, a blood compatibility test was performed to determine if the PDs induce hemolysis in mice[25]. As shown in Fig. 3b, no hemolysis of red blood cells was caused by the PDs, even at a concentration of 4000 μg/mL, indicating favorable blood compatibility. Thus, the cellular experiments and hemolysis assay confirmed the biocompatibilities of the PDs, especially in comparison with PEI alone, the cytotoxicity of which has been cited as a significant concern in the literature[26].

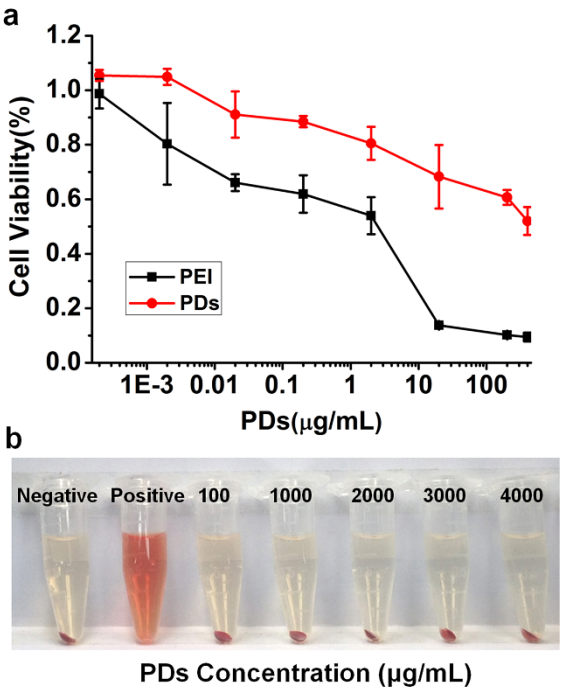

Figure 3 | (a) Cytotoxicity of the PDs and PEI alone. (b) Hemolysis test with different concentrations of the PDs (negative: phosphate buffer solution; positive: dd H_2O).

***In vitro* and *in vivo* imaging.** We next evaluated the possibility of using the PDs as fluorescence probes for *in vitro* and *in vivo* imaging. Significant luminescence of the PDs was observed in MCF-7 cells using excitation wavelengths of 405, 488 and 543 nm (Fig. 4a). For further imaging analysis *in vivo*, we firstly observed the spectra of the PDs using a Maestro *in vivo* optical imaging system. As shown in Fig. 4b, the PDs showed concentration-dependent fluorescence in all three excitation filters tested, and the green filter (excited at 503–548 nm) yielded the strongest fluorescence intensity. Longer infrared wavelengths are most suitable for *in vivo* imaging, but the fluorescence intensity decreased markedly using the red filter (excited at 616–661 nm). We therefore chose the green filter for further *in vivo* imaging analysis. Subcutaneous and intramuscular injections of PDs were administered to the right flank of two nude mice. As shown in Fig. 4c, although the near-skin fluorescence intensity is higher than the signal emanating from deeper tissue, bright emissions were detected in fluorescence images of both injection sites. Unfortunately, the fluorescence of PDs could not be clearly detected in live mouse after intravenous injection. Furthermore, biodistribution studies on organs collected at multiple time points after intravenous injection were carried out (Fig. 4d). Liver showed the strongest fluorescence signals, and the specific signals last for at least 24 h. Although lungs showed the moderate signals, the signals were cleared very quickly (within 2 h). These results indicate that the intrinsic luminescence can potentially be used for monitoring biodistribution of the PDs in live animals as well as microscopic observation of their localization in organs.

Combined drug delivery and imaging of PDs into tumors. We wanted to demonstrate the unique drug delivery features of the

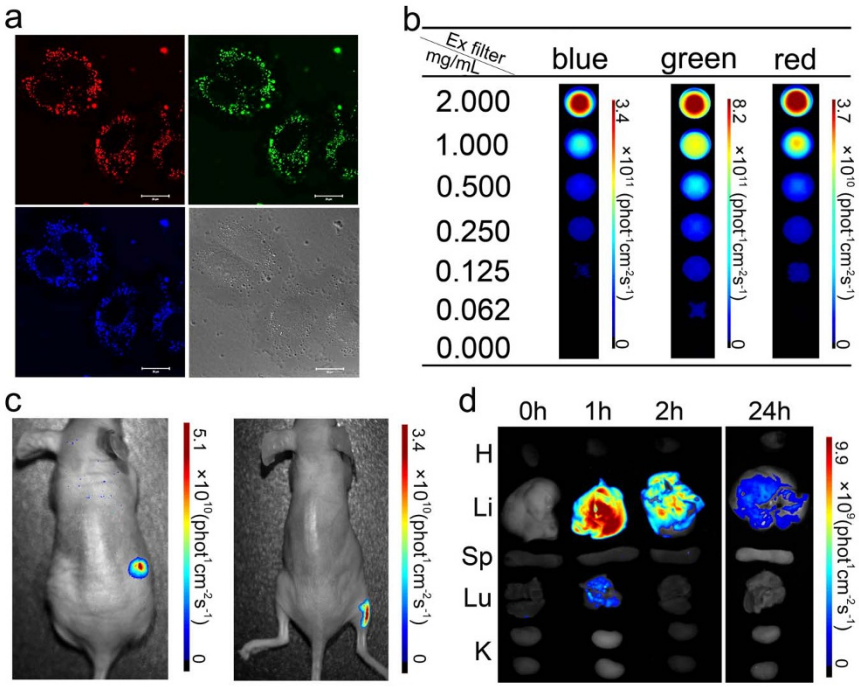

Figure 4 | (a) In vitro cellular imaging of PDs. MCF-7 cells were treated with PDs for 4 h and then imaged with excitation wavelengths of 405, 488 and 543 nm. The scale bar is 20 μm. (b) Fluorescence images of PDs as a function of concentration using a Maestro in vivo imaging system with different excitation filters (blue: 435–480 nm; green: 503–548 nm; red: 616–661 nm). Ex filter: excitation filter. (c) In vivo fluorescence image of PDs (20 μl of 2 mg/mL) injected into mice subcutaneously (left) and intramuscularly (right). (d) Fluorescence images showing the ex-vivo biodistribution of PDs in organs collected from the animals at the time points shown after intravenous injection. Li, liver; Sp, spleen; K, kidney; H, heart; Lu, lung.

PDs, which potentially make them powerful theranostic vehicles for imaging-guided drug delivery. First, we tested whether the PEI-containing PDs retained the proton-buffering ability of PEI alone[27]. Fig. S6 shows that the PEI-containing PDs have broad proton-buffering ability within the endosomal pH range (specifically at pH 5.1–7.4), similar to PEI alone at an equal concentration of amine groups. However, the buffering capacity of PDs (10.3%) was lower than PEI alone (average 17.9% from two different concentrations). The broad proton-buffering ability should allow the PDs to escape easily from endosomes/lysosomes, where many drug delivery vehicles become trapped and are unable to release the drug to cytoplasm[28]. Then we carried out confocal experiments at various time points and analyzed the co-occurrence between PDs and endosomes/lysosomes using a method as previously reported[29]. Consistently, compared to the data when treated for 0.5 h and 1 h, the fluorescent signal of PDs in cells treated for 4 h did not co-localize with the endosomes/lysosomes (dyed with lysotracker red), indicating that the PDs had already escaped to the cytoplasm from endosomes/lysosomes (Fig. S7a,b).

We next investigated the degree of drug release and inhibition of cell growth *in vitro* and further assessed the therapeutic potential of the drug-loaded PDs *in vivo*. The representative drug, Paclitaxel (PTX), was encapsulated within the hydrophobic core of the PDs using the modified emulsion/solution methods[21]. The optimal loading content and encapsulation efficiency of PTX-loaded PDs were 5.11 ± 0.26 wt.% and 61.7 ± 3.5%, respectively (Table S1). The PTX-loaded PDs and blank PDs exhibited no obvious difference in size and were highly stable in different solutions (Table S2). Drug release experiments showed that in both acidic conditions (pH 5.2) and physiological conditions (pH 7.4) there was an initial burst of PTX release from the PDs within the first 12 hours, followed by sustained release (Fig. 5a). However, PTX was released much faster at pH 5.2 than that at pH 7.4, indicating that the PTX-loaded PDs have a pH-sensitive release profile. This pH sensitivity may benefit the release of PTX when drug-loaded PDs enter the acidic endosome/lysosome compartments of cells. Fig. 5b shows cell viabilities after incubating with free PTX, blank PDs and PTX-loaded PDs for 48 h. PTX-loaded PDs were more cytotoxic than free PTX, whereas blank PDs showed no significant cytotoxicity.

We next compared the *in vivo* antitumor activity of PTX-loaded PDs with free PTX and saline. Both free PTX and PTX-loaded PDs effectively inhibited MCF-7 tumor growth, whereas the tumor growth rate of mice treated with PTX-loaded PDs was much lower than that of the free PTX-treated mice (Fig. 5c). The average tumor weight in the group treated with PTX-loaded PDs was significantly decreased in contrast to the free PTX group (Fig. 5d). Meanwhile, the excised tumors from the mice after intravenous injection with PTX-loaded PDs showed obvious fluorescence in contrast to the saline group, which indicated the accumulation of PTX-loaded PDs in the tumors (Fig. 5e). In addition, the body weight of tumor-bearing mice treated with PTX-loaded PDs did not change significantly during the treatment period compared to the other two groups (Fig. S8a), which was consistent with the biocompatibility of the PDs (Fig. 3a,b). Representative images of excised tumors from mice receiving different treatments are shown in Fig. S8b. Overall, PTX-loaded PDs exhibited significantly higher antitumor activity than free PTX and can be used as an effective drug delivery system for cancer treatment.

Discussion

In this work, we report herein novel, multifunctional PDs that have the potential to be used as imaging-guided drug delivery vehicles as part of a "see and treat" strategy. Originally, the PEI-PLA copolymer was designed to improve the biocompatibility of PEI. Interestingly, the PEI-PLA copolymer-based nanoparticles showed unique ultrabright and multicolorful fluorescence property. PDs based on PEI-PLA copolymer show an excitation-dependent fluorescence behavior, and significant red-shift of PDs. Meanwhile, we find that PEI show negligible fluorescence when excited at wavelengths above 420 nm. Lourdes et al.[23] indicated that the fluorescence of PEI was attributed

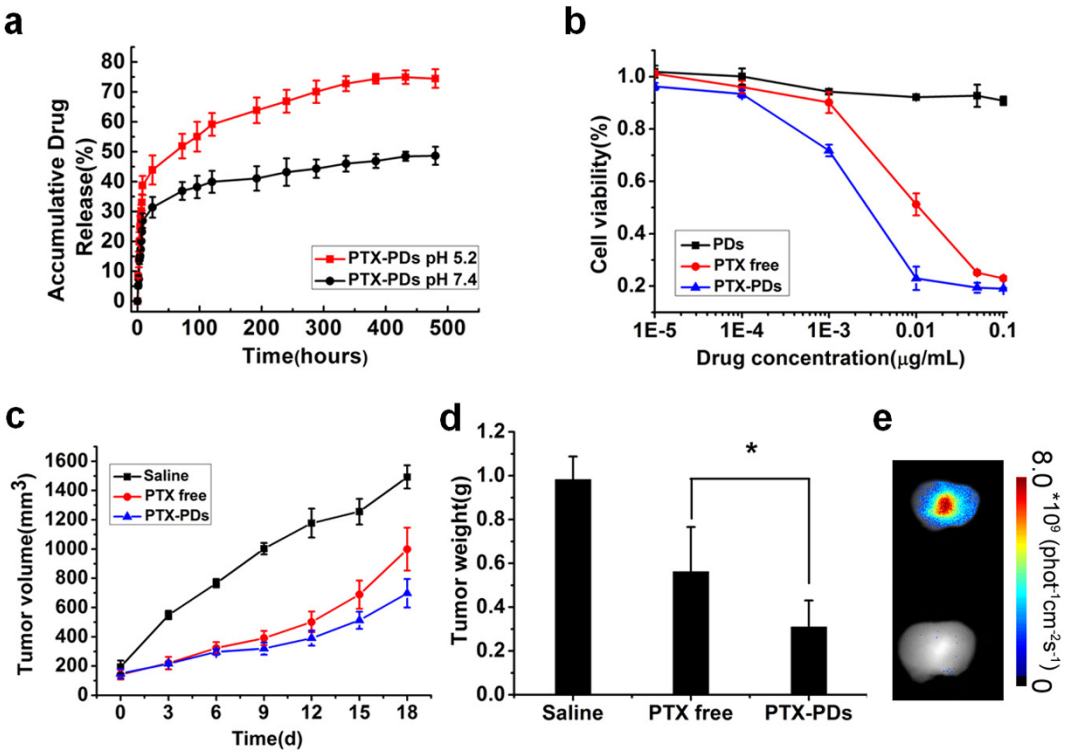

Figure 5 | (a) In vitro drug release of PTX-loaded PDs in acidic conditions (pH 5.2) and physiological conditions (pH 7.4). (b) Cytotoxicity of free PTX, PTX-loaded PDs, and blank PDs after 48 h incubation with MCF-7 cells. The concentration of blank PDs used was equal to the concentration of PTX-loaded PDs. (c, d) Tumor volume and tumor weight of MCF-7 tumor-bearing female nude mice treated with saline, PTX or PTX-loaded PDs. *,$P<0.05$.(e) Fluorescence images showing the ex-vivo biodistribution of PDs in tumors isolated from the mice after intravenous injection. Lower, saline group; Upper, PTX-loaded PDs group.

to amine rich nano-clusters and electro-hole recombination. PLA nanoparticles with no polyamine (such as PEG-PLA) have rarely been demonstrated their fluorescence. Our lab has previously synthesized the amphiphilic fluorescent copolymer based on HPAE-PLA[30]. The copolymer and self-assembled nanoparticles exhibited similar excitation-dependent fluorescence behaviour as the PEI-based PDs. The HPAE prepared by Dengchen Wu just showed blue fluorescence[31], but the nanoparticles based on the amphiphilic HPAE-PLA copolymer demonstrated obvious green emission when excited at 455 nm using the laser scanning confocal microscopy. This result evidenced that the rigid and compact structure of the HPAE-PLA nanoparticles played a very important role for red-shift of the fluorescence emission from blue to green. The enhanced fluorescence of PEI-PLA nanoparticle (Fig. 2d) and PEI-PLA copolymer powder (Fig. S3) demonstrate that the rigid and compact structure of the PDs played a crucial role in the excitation-dependent and enhance fluorescence behavior. Previous studies[10] have demonstrated that the conformation of PAMAM was pH-responsive and the acidic environment could form the much more rigid and compact conformation. To further investigate the potential mechanism for the multicolor and enhanced fluorescence of PDs, we further study the fluorescence intensity of the PDs with the emission at 450 nm and 540 nm at different pH. The pH-dependent fluorescence of PDs (Fig. S4) further confirm that the acidic environment result in the much more rigid and compact conformation and induce the unique fluorescent effect.

In order to check the biocompatibility of PDs, we carry out the CCK-8 assay and hemolysis assay to demonstrate that the PDs possess a good biocompatibility compared with PEI. And the biocompatibility of PDs further promotes the development of PDs in nanomedicine. The ultrabright and near-infrared fluorescence of PDs make them suitable for *in vitro* (Fig. 4a) and *in vivo* (Fig. 4c, d) imaging. The drug release study confirms that the PTX-loaded PDs show a controlled and pH-responsive drug-release profile. The PTX-loaded PDs was effective in inhibiting tumor cell growth at low concentration *in vitro*. Furthermore, in vivo tumor growth inhibition study was performed in nude mice with MCF-7 tumor revealed that the pH-sensitive PTX-loaded PDs significantly suppress the tumor growth. Meanwhile, the body weight of tumor-bearing mice treated with PTX-loaded PDs did not change significantly during the treatment period compared to the other two groups (Fig. S8a). These results revealed that the great potential of the unique multicolorful PDs design in imaging guided drug delivery applications.

In conclusion, this work represents the first proof of concept that the multifunctional PDs possessing excitation-dependent fluorescence behavior and multicolorful fluorescence to be used as imaging-guided drug delivery vehicles. The ultrabright and near-infrared fluorescence of PDs make them suitable for *in vitro* and *in vivo* imaging. This study represents the first example of *in vitro* and *in vivo* imaging using biocompatible PEI-containing PDs in live animals. More importantly, the PTX-loaded PDs showed a controlled and pH-responsive drug-release profile that was effective in inhibiting tumor cell growth at low concentration *in vitro*. Cell and animal studies revealed the great potential of the pH-sensitive PEI-containing PDs for therapeutic effect in cancer treatment.

Methods

Reagents and cell lines. Branched polyethyleneimine (PEI, 25 kD) was obtained from Sigma-Aldrich (St. Louis, MO, USA). D,L-Lactide (DLLA), was obtained from Alfa Aesar (Ward Hill, MA, USA). Paclitaxel (PTX) was purchased from NuoRi Co, Ltd. (Beijing, China). Human breast adenocarcinoma (MCF-7) cells were purchased from the American Type Culture Collection (ATCC; Manassas, VA, USA). CCK-8 Kits were purchased from Dojindo Molecular Technologies (Japan). All other reagents and solvents were of analytical grade.

Synthesis of PEI-PLA copolymers. Pre-dehydrated (15 g, 10 g and 5 g) DLLA and (0.25 g) PEI were dissolved in 50 mL anhydrous dimethylsulfoxide by stirring,

respectively, and then 0.05 mol triethylamine was added. The solution was kept at 86°C with constant stirring under nitrogen for 12 h. Subsequently, the reacted solution was added to ice-water and the precipitate collected and thoroughly washed with distilled water. Finally, the obtained product was extracted using toluene to remove homopolymer.

Preparation of PDs. In brief, 20 mg of PEI-PLA copolymers and a given amount of PTX were dissolved in 2 mL dichloromethane. The mixture was then slowly added to 10 mL aqueous solution with 1–4% (w/v) of polyvinyl alcohol (PVA) under gentle stirring for 10 min. The emulsion was then sonicated for 5 min at 40 W and then evaporated under reduced pressure to remove the dichloromethane. After that, the PDs suspension was centrifuged at 15,000 rpm for 15 min and washed with deionized water three times.

***In vitro* and *in vivo* fluorescence imaging.** For the *in vitro* imaging, MCF-7cells were cultured in DMEM medium containing PDs for 4 h in confocal dishes. The cells were then imaged with a laser confocal scanning microscope (Zeiss) equipped with a 60× oil immersion lens. The excitation wavelengths were 405, 488 and 543 nm. To minitor the colocalization between PDs and endosomes/lysosomes, MCF-7cells were stained with lysotracker red (Molecular Probes, USA) after culturing in DMEM medium containing PDs for various times. Then the cells were imaged by confocal microscopy and the data were analysed according to the method described before[29].

For the *in vivo* imaging, mice were injected subcutaneously and intramuscularly in the right flank with blank PDs respectively and imaged immediately with green excitation (503–548 nm) using the Maestro in vivo optical imaging system. For systemic administration, blank PDs were intravenously injected into nude mice (20 mg/kg). The mice were imaged under anesthesia several different times after injection using the Maestro in vivo optical imaging system. The organs (heart, kidney, liver, lung and spleen), collected at multiple time points after injection, were also imaged.

Cytotoxicity assays. MCF-7 cells were seeded at a density of 5×10^3 cells per well in 96-well plates in DMEM medium and incubated for 24 h. The medium was then replaced with 200 μL of medium containing various equivalent concentrations of blank PDs and PEI; or blank PDs, free-PTX and PTX-loaded PDs. The cells were incubated for 48 h and cytotoxicity assays were performed using CCK-8 Kits (Dojindo Molecular Technologies, Tokyo, Japan). All data were presented as mean percentages ± SEM in triplicate compared to the OD values of untreated cells.

***In vivo* therapeutic efficacy.** Female nude mice (18–20 g) were purchased from Beijing Vital River Company (Beijing, China) and housed under standard conditions with free access to food and water. All animal experiments were performed in accordance with the principles of care and use of laboratory animals. Next, 2×10^6 MCF-7 cells in 100 μL of physiological saline were injected subcutaneously into the right flank of nude mice. The animals were randomly divided into 3 groups (five mice per group) and when the tumors reached about 100 mm^3 they were treated with saline, free PTX (10 mg/kg) or PTX-loaded PDs (administered at a PTX-equivalent dose of 10 mg/kg). Drugs were administered by intravenous (i.v.) injection every 3 days for a total of seven times. Tumor progression in the mice was then monitored every three days. Tumor volumes were calculated as (length × $width^2$)/2 (mm^3). The mice were sacrificed at the end of the experiment, and their tumors were immediately removed and weighed. All of the animal experiments were conducted under approved protocols of the Institutional Animal Care and Use Committee at the Institute of Tumor in the Chinese Academy of Medical Science.

1. Petros, R. A. & DeSimone, J. M. Strategies in the design of nanoparticles for therapeutic applications. *Nat. Rev. Drug Discov.* **9**, 615–627 (2010).
2. Howes, P. *et al.* Magnetic Conjugated Polymer Nanoparticles as Bimodal Imaging Agents. *J. Am. Chem. Soc.* **132**, 9833–9842 (2010).
3. Ma, K., Sai, H. & Wiesner, U. Ultrasmall Sub-10 nm Near-Infrared Fluorescent Mesoporous Silica Nanoparticles. *J. Am. Chem. Soc.* **134**, 13180–13183 (2012).
4. Panyam, J. & Labhasetwar, V. Biodegradable nanoparticles for drug and gene delivery to cells and tissue. *Adv. Drug Del. Rev.* **55**, 329–347 (2012).
5. Resch-Genger, U., Grabolle, M., Cavaliere-Jaricot, S., Nitschke, R. & Nann, T. Quantum dots versus organic dyes as fluorescent labels. *Nat. Methods* **5**, 763–775 (2008).
6. Brown, S. D. *et al.* Gold nanoparticles for the improved anticancer drug delivery of the active component of oxaliplatin. *J. Am. Chem. Soc.* **132**, 4678–4684 (2010).
7. Lee, J. H. *et al.* Artificially engineered magnetic nanoparticles for ultra-sensitive molecular imaging. *Nat. Med.* **13**, 95–99 (2006).
8. Duncan, R. Polymer conjugates as anticancer nanomedicines. *Nat. Rev. Cancer* **6**, 688–701 (2006).
9. Dhar, S., Gu, F. X., Langer, R., Farokhzad, O. C. & Lippard, S. J. Targeted delivery of cisplatin to prostate cancer cells by aptamer functionalized Pt(IV) prodrug-PLGA-PEG nanoparticles. *Proc. Natl. Acad. Sci. U S A* **105**, 17356–17361 (2008).
10. Chen, W., Tomalia, D. A. & Thomas, J. L. Unusual pH-Dependent Polarity Changes in PAMAM Dendrimers: Evidence for pH-Responsive Conformational Changes. *Macromolecules* **33**, 9169–9172 (2000).
11. Derfus, A. M., Chan, W. C. W. & Bhatia, S. N. Probing the cytotoxicity of semiconductor quantum dots. *Nano Lett.* **4**, 11–18 (2004).
12. Moon, J. H., McDaniel, W., Maclean, P. & Hancock, L. F. Live-cell-permeable poly(p-phenylene ethynylene). *Angew. Chem. Int. Ed.* **46**, 8223–8225 (2007).
13. Yang, B., Zhu, S., Zhang, J. & Wang, H. Y. A general route to make non-conjugated linear polymer luminescent. *Chem. Commun.* **48**, 10889–10891 (2012).
14. Howes, P., Green, M., Levitt, J., Suhling, K. & Hughes, M. Phospholipid Encapsulated Semiconducting Polymer Nanoparticles: Their Use in Cell Imaging and Protein Attachment. *J. Am. Chem. Soc.* **132**, 3989–3996 (2010).
15. Wu, C. *et al.* Ultrabright and bioorthogonal labeling of cellular targets using semiconducting polymer dots and click chemistry. *Angew. Chem. Int. Ed.* **49**, 9436–9440 (2010).
16. Wu, C. *et al.* Bioconjugation of Ultrabright Semiconducting Polymer Dots for Specific Cellular Targeting. *J. Am. Chem. Soc.* **132**, 15410–15417 (2010).
17. Wu, C. *et al.* Design of highly emissive polymer dot bioconjugates for in vivo tumor targeting. *Angew. Chem. Int. Ed.* **50**, 3430–3434 (2011).
18. Varkouhi, A. K., Scholte, M., Storm, G. & Haisma, H. J. Endosomal escape pathways for delivery of biologicals. *J. Control. Release* **151**, 220–228 (2011).
19. Mishra, D., Kang, H. C. & Bae, Y. H. Reconstitutable charged polymeric (PLGA)2-b-PEI micelles for gene therapeutics delivery. *Biomaterials* **32**, 3845–3854 (2011).
20. Han, S. *et al.* Efficient Delivery of Antitumor Drug to the Nuclei of Tumor Cells by Amphiphilic Biodegradable Poly(L-Aspartic Acid-co-Lactic Acid)/DPPE Co-Polymer Nanoparticles. *Small* **8**, 1596–1606 (2012).
21. Xu, Q. *et al.* Anti-tumor activity of paclitaxel through dual-targeting carrier of cyclic RGD and transferrin conjugated hyperbranched copolymer nanoparticles. *Biomaterials* **33**, 1627–1639 (2012).
22. Lee, Y. *et al.* Controlled synthesis of PEI-coated gold nanoparticles using reductive catechol chemistry for siRNA delivery. *J. Control. Release* **155**, 3–10 (2011).
23. Pastor-Perez, L., Chen, Y., Shen, Z., Lahoz, A. & Stiriba, S-E. Unprecedented blue intrinsic photoluminescence from hyperbranched and linear polyethylenimines: Polymer architectures and pH-effects. *Macromol. Rapid Commun.* **28**, 1404–1409 (2007).
24. Liu, J. *et al.* Hyperbranched Conjugated Polysiloles: Synthesis, Structure, Aggregation-Enhanced Emission, Multicolor Fluorescent Photopatterning, and Superamplified Detection of Explosives. *Macromolecules* **43**, 4921–4936 (2010).
25. Dobrovolskaia, M. A. *et al.* Method for Analysis of Nanoparticle Hemolytic Properties in Vitro. *Nano Lett.* **8**, 2180–2187 (2008).
26. Vancha, A. R. *et al.* Use of polyethyleneimine polymer in cell culture as attachment factor and lipofection enhancer. *BMC Biotechnol.* **4**, 23 (2004).
27. Mishra, D., Kang, H. C. & Bae, Y. H. Reconstitutable charged polymeric (PLGA)(2)-b-PEI micelles for gene therapeutics delivery. *Biomaterials* **32**, 3845–3854 (2011).
28. Akinc, A., Thomas, M., Klibanov, A. M. & Langer, R. Exploring polyethylenimine-mediated DNA transfection and the proton sponge hypothesis. *J. Gene Med.* **7**, 657–663 (2005).
29. Adler, J. & Parmryd, I. Colocalization analysis in fluorescence microscopy. *Methods Mol Biol.* **931**, 97–109 (2013).
30. Miao, Q. *et al.* Amphiphilic hyper-branched co-polymer nanoparticles for the controlled delivery of anti-tumor agents. *Biomaterials* **31**, 7364–7375 (2010).
31. Wu, D. C., Liu, Y., He, C. B. & Goh, S. H. Blue photoluminescence from hyperbranched poly(amino ester)s. *Macromolecules* **38**, 9906–9909 (2005).

Acknowledgements

This work was supported by the Ministry of Science and Technology of China (2009CB930200), National Natural Science Foundation of China (30970784, 81171455, and 81272453).

Author contributions

Y.S., W.P.C., Y.W. and X.J.L. designed the research. Y.S., W.P.C., S.L.L., K.L.H. and Y.Y.H. carried out the experiments. Y.S., W.P.C., S.L.L., X.Y.G., L.M.H., Y.W. and X.J.L. analyzed data and participated in the discussion. Y.S., W.P.C., S.L.L., S.B.J., Y.W. and X.J.L. wrote and revised the paper. All authors reviewed the manuscript.

Additional information

Supplementary information accompanies this paper at http://www.nature.com/scientificreports

Competing financial interests: The authors declare no competing financial interests.

How to cite this article: Sun, Y. *et al.* Ultrabright and Multicolorful Fluorescence of Amphiphilic Polyethyleneimine Polymer Dots for Efficiently Combined Imaging and Therapy. *Sci. Rep.* **3**, 3036; DOI:10.1038/srep03036 (2013).